Received: 27 February 2021 | Accepted: 6 May 2021

DOI: 10.1002/stem.3428

TISSUE-SPECIFIC STEM CELLS

STEM CELLS®

DUSP5 promotes osteogenic differentiation through SCP1/2-dependent phosphorylation of SMAD1

Xuejiao Liu[1,2] | Xuenan Liu[1,2] | Yangge Du[1,2] | Menglong Hu[1,2] | Yueming Tian[1,2] | Zheng Li[1,2] | Longwei Lv[1,2] | Xiao Zhang[1,2] | Yunsong Liu[1,2] | Yongsheng Zhou[1,2] | Ping Zhang[1,2]

[1]Department of Prosthodontics, School and Hospital of Stomatology, Peking University, Beijing, People's Republic of China

[2]National Engineering Lab for Digital and Material Technology of Stomatology, National Clinical Diseases, Peking University School and Hospital of Stomatology, Peking University, Beijing, People's Republic of China

Correspondence

Yongsheng Zhou, DDS, PhD, Vice Dean of the School, Chair and Professor of Department of Prosthodontics, Peking University School and Hospital of Stomatology, 22 Zhongguancun South Avenue, Haidian District, Beijing 100081, People's Republic of China.
Telephone: 86-1082195370;
Email: kqzhouysh@hsc.pku.edu.cn

Ping Zhang, PhD, Department of Prosthodontics, Peking University School and Hospital of Stomatology, 22 Zhongguancun South Avenue, Haidian District, Beijing 100081, People's Republic of China.
Telephone: 86-10-82195370;
Email: zhangping332@hsc.pku.edu.cn

Funding information

Beijing Natural Science Foundation, Grant/Award Number: 7202233; Capital Culturing Project for Leading Talents in Scientific and Technological, Innovation in Beijing, Grant/Award Number: Z171100001117169; National Natural Science Foundation of China, Grant/Award Numbers: 81870742, 81970911

Abstract

Dual-specificity phosphatases (DUSPs) are defined by their capability to dephosphorylate both phosphoserine/phosphothreonine (pSer/pThr) and phosphotyrosine (pTyr). DUSP5, a member of DUSPs superfamily, is located in the nucleus and plays crucially regulatory roles in the signaling pathway transduction. In our present study, we discover that DUSP5 significantly promotes osteogenic differentiation of mesenchymal stromal cells (MSCs) by activating SMAD1 signaling pathway. Mechanistically, DUSP5 physically interacts with the phosphatase domain of small C-terminal phosphatase 1/2 (SCP1/2, SMAD1 phosphatases) by the linker region. In addition, we further confirm that DUSP5 activates SMAD1 signaling through a SCP1/2-dependent manner. Specifically, DUSP5 attenuates the SCP1/2-SMAD1 interaction by competitively binding to SCP1/2, which is responsible for the SMAD1 dephosphorylation, and thus results in the activation of SMAD1 signaling. Importantly, DUSP5 expression in mouse bone marrow MSCs is significantly reduced in ovariectomized (OVX) mice in which osteogenesis is highly passive, and overexpression of *Dusp5* via tail vein injection reverses the bone loss of OVX mice efficiently. Collectively, this work demonstrates that the linker region of DUSP5 maybe a novel chemically modifiable target for controlling MSCs fate choices and for osteoporosis treatment.

KEYWORDS

DUSP5, osteogenesis, osteoporosis, SCP1/2, SMAD1 signaling

Significance statement

DUSP5 plays a crucially regulatory role in the signaling pathway transduction by dephosphorylating phosphoserine/phosphothreonine (pSer/pThr) and phosphotyrosine. However, whether DUSP5 participates in osteogenesis and the underling mechanisms remains unclear. This study demonstrates that DUSP5 promotes mesenchymal stromal cells osteoblastic differentiation by activating SMAD1 signaling in a SCP1/2-dependent manner, and the linker region of DUSP5 maybe the novel chemically modifiable target for controlling MSCs fate choices and for osteoporosis treatment.

1 | INTRODUCTION

Many signaling cascades are initiated and controlled by kinases, which supports the notion that protein phosphorylation provides a common language in activating and modulating signal transduction. Bone morphogenetic protein (BMP)/SMAD signaling transduction cascade is initiated by ligands-serine/threonine kinase receptor (type I: BMPR1A and BMPR1B; type II: BMPR2) complex, following the phosphorylation of receptor-related SMADs (R-SMADs, SMAD1, 5, and 8/9). Phosphorylated SMADs then recruit chromatin-remodeling machinery and transcription factors to the genomics to regulate gene expressions, which plays an essential role in a myriad of cellular activities, including proliferation, recognition, differentiation, apoptosis, and cell-fate specification.[1-4] In vertebrates, BMP/SMAD signaling directs mesenchymal differentiation along osteogenic lineage by targeting transcription factors, such as runt-related transcription factor 2 (*Runx2*) and osterix (*Osx*).[5-7]

The discovery of phosphatases indicates that protein phosphorylation is reversible, allowing for greater plasticity of signal transduction controlled by substrate phosphorylation. In nucleus, phosphatases toward the dephosphorylation of R-SMADs are of great importance to prevent excessive activation of SMAD signaling. SMADs phosphatases, including Mg^{2+}/Mn^{2+}-dependent 1A phosphatase (PPM1A; also known as PP2C),[8,9] pyruvate dehydrogenase phosphatase (PDP),[10] and small C-terminal domain phosphatases (SCPs, also known as CTDSP),[11,12] could terminate SMAD signaling pathway by dephosphorylating and promoting nuclear export of SMADs. SCPs belong to a family of Mg^{2+}-dependent phosphoserine/phosphothreonine (pSer/pThr)-specific phosphatases and are originally reported to dephosphorylate the C-terminal domain (CTD) of RNA polymerase II by aspartic acids of the sequence motif DxDxT/V.[13,14] Recently, SCPs have been shown to regulate mesenchymal differentiation by suppressing BMP/TGFβ signaling in a manner of SMADs C-terminal or linker regions dephosphorylation.[11,15,16]

The dual-specificity phosphatases (DUSPs) is another kind of phosphatases superfamily characterized by dephosphorylating both threonine/serine and tyrosine residues of their substrates.[17,18] Many investigations indicate that DUSPs are involved in cancers,[19-26] diabetes,[27-30] cardiovascular disorders,[31-33] and immune inflammatory diseases.[34-37] Besides, DUSP1 and DUSP2 are proposed to inhibit osteoclastic bone resorption.[38] DUSP5/HVH3, a member of DUSPs family, is located in nucleus and has been reported to deactivate specifically to extracellular signal-related kinases (ERKs), and the presence of a secondary binding site and a disulfide bridge renders DUSP5 highly specific toward bi-phosphorylated ERK (pTpY-ERK).[39-41] In autoimmune arthritis or inflammatory osteoarthritis, DUSP5 could attenuate bone loss,[42,43] indicating that DUSP5 may be a potential regulator for osteoblast function.

In the present study, we uncovered a novel role of DUSP5 in human mesenchymal stem cells (hMSCs) osteogenic differentiation by activating SMAD1 signaling. Unlike functioning toward its well-known substrate ERKs, DUSP5 was firstly discovered to interact with the SMAD1 phosphatases SCP1/2 and activate SMAD1 signaling through a SCP1/2-dependent manner. We clarified that the linker region of DUSP5 associated with and occupied the phosphatase domain of SCP1/2, thus inhibiting the dephosphorylation effect of SCP1/2 on SMAD1. Moreover, *Dusp5* overexpression significantly improved the osteogenic differentiation potential of mouse bone marrow mesenchymal stromal cells (mBMMSCs), and reversed the bone loss of ovariectomized (OVX) mice. Collectively, our data demonstrated an unexpected role of DUSP5 in MSCs osteoblastic commitment through SCP1/2-dependent modulation of SMAD1 signaling and presented that DUSP5 might be a potential target for osteoporosis treatment.

2 | MATERIALS AND METHODS

2.1 | Cell culture

hMSCs from 3 healthy adult donors used in our study were obtained from ScienCell Research Laboratory (Carlsbad, California), and 3-6 passages were used in our experiment. Materials for cell culture were from Sigma-Aldrich (St. Louis, Missouri). hMSCs were cultured in proliferation medium (PM) which was consisted of Minimum Essential Medium α (α-MEM, Gibco, Grand island, Nebraska)/Dulbecco's modified Eagle's medium (DMEM, Gibco, Grand island, Nebraska), fetal bovine serum (FBS; 10%, vol/vol), penicillin G (100 U/mL), and streptomycin (100 mg/mL) and osteogenic medium (OM) which was supplemented with 100 nM Dexamethasone, 0.2 mM L-ascorbic acid, and 10 mM β-glycerophosphate on the basis of PM. mBMMSCs were flushed out of femurs of C57BL/6 mice which were bought from Charles River Corporation (Beijing, China), and were cultured in α-MEM mixed with 20% FBS and 2% antibiotics. The cell culture conditions were a humidified atmosphere of 95% air, 5% CO_2, and 37°C.

2.2 | Lentiviral transfection

Lentiviruses targeting *DUSP5* (sh*DUSP5*-1, sh*DUSP5*-2, sh*DUSP5*-3) and negative control (NC); *DUSP5*-overexpressing lentivirus (*DUSP5*) and vector were purchased from GenePharma Co. (Suzhou, China). The sequences of sh*DUSP5*-1, sh*DUSP5*-2, sh*DUSP5*-3, and NC are listed in Table 1. For construction of *DUSP5* rescue cell lines, sh*DUSP5* cells were transfected with lentivirus of vector or *DUSP5* (*DUSP5*, GenePharma Co.). When cell fusion rate reaches 40%-50%, viral suspension with 5 mg/mL polybrene (Sigma) was added into the cell culture. Puromycin (1 μg/mL, Sigma-Aldrich) was applied to screening the stably transfected cells after transfection 72-96 hours.

2.3 | RNA interference and plasmid transfection

The sequences of short-interfering (si) RNAs targeting *SMAD1* (si*SMAD1*), *SCP1* (si*SCP1*), *SCP2* (si*SCP2*), and the Negtive Control (NC) were listed in Table 1. Plasmids include pcDNA3.1-DUSP5 (addgene: #70325), pGEX-6p-1-DUSP5, pcDNA3.1-SCP1, pcDNA3.1-SCP2,

TABLE 1 Sequences of DNA oligonucleotides and RNA

Name	Sense strand/sense primer (5′-3′)	Antisense strand/antisense primer (5′-3′)
shRNA		
N C	TTCTCCGAACGTGTCACGT	
sh*DUSP5*-1	GGCCTTCGATTACATCAAG	
sh*DUSP5*-2	GAGAAGATTGAGAGTGAGA	
sh*DUSP5*-3	GCAATAGACTTCATTGACTGT	
si-RNA		
NC	UUCUCCGAACGUGUCACGUTT	ACGUGACACGUUCGGAGAATT
si*SMAD1*	GGUGCUCUAUUGUCUACUATT	UAGUAGACAAUAGAGCACCTT
si*SCP1*	CCUCGUGGUUUGACAACAUGATT	UCAUGUUGUCAAACCACGAGGTT
si*SCP2*	GCCUCGUGGACGUAACAUCUUTT	AAGAUGUUACGUCCACGAGGCTT
Primers		
OSX	CCTCCTCAGCTCACCTTCTC	GTTGGGAGCCCAAATAGAAA
RUNX2	CCGCCTCAGTGATTTAGGGC	GGGTCTGTAATCTGACTCTGTCC
DUSP5	CCTGAGTGTTGCGTGGATGT	ACTGGGCCACCCTGGTCATAA
GAPDH	GGAGCGAGATCCCTCCAAAAT	GGCTGTTGTCATACTTCTCATGG
Osx	GTCCTCTCTGCTTGAGGAAGAA	TCTTTGTGCCTCCTTTCCCC
Runx2	CCGCACGACAACCGCACCAT	CGCTCCGGCCCACAAATCTC
Dusp5	ACCAGCCTATGACCAGGGTG	GGAACTCGCACTTGGATGCG
Gapdh	ACCACAGTCCATGCCATCAC	TCCACCACCCTGTTGCTGTA

Abbreviations: *DUSP5*, dual-specificity phosphatases 5; *GAPDH*, glyceraldehyde 3-phosphate dehydrogenase; NC, negative control for sh*DUSP5*-1, sh*DUSP5*-2, and sh*DUSP5*-3; *OSX*, osterix; *RUNX2*, runt-related transcription factor 2; SCP, small C-terminal phosphatase; shRNA, short-hairpin RNA; si-RNA, short-interfering RNA; *SMAD1*, mall mothers against decapentaplegic.

pcDNA3.1-Flag-DUSP5, pcDNA3.1-HA-DUSP5 (1-140), pcDNA3.1-HA-DUSP5 (1-178), pcDNA3.1-HA-DUSP5 (179-384), pcDNA3.1-HA-DUSP5 (141-384), pcDNA3.1-Myc-SCP1, pcDNA3.1-Myc-SCP1 (1-88), pcDNA3.1-Myc-SCP1 (89-232), and pcDNA3.1-Myc-SCP1 (89-261) and vectors. Both siRNAs and plasmids were purchased from Sangon Biotech (Shanghai, China), and transfected by Lipofectamine 3000 according to the manufacturer's introduction (Invitrogen, Carlsbad, California). 48 hours after transfection, cells were collected to analyze the gene expressions. During the process of osteo-induction, transfection was repeated every 2-3 days to ensure transfection efficiency.

2.4 | Alkaline phosphatase staining and quantification

hMSCs were seeded in 6-well or 12-well plates. After 7 days of osteo-induction, cells were fixed in 95% cold ethanol for 30 minutes, followed by 3 times of rinses with phosphate-buffered saline (PBS). Then, ALP staining and quantification were conducted according to the manufacturer's instructions. ALP staining kit (Biyuntian, Shanghai, China), bicinchoninic acid (BCA) protein assay kit (Pierce Thermo Scientific, Waltham, Massachusetts), and ALP assay kit (Nanjing Jiancheng Bioengineering Institute, Nanjing, China) were used. ALP staining images were scanned, and the absorbance of solution for ALP quantification was measured at 520 nm and normalized to the total protein concentration.

2.5 | Alizarin red S staining and quantification

For ARS staining and quantification, cells were seeded in 6-well or 12-well plates. On the 14th day of osteogenesis induction, cells were fixed with 95% ethanol for 30 minutes. After washed with distilled water for 3 times, the cells were incubated with ARS solution (2%, pH 4.2, Sigma-Aldrich). For quantification, the plate was incubated with 100 mM cetylpyridinium chloride (Sigma-Aldrich) for 1 hour and the solution was collected. ARS staining images were scanned, and the absorbance of solution for ARS quantification was measured at 562 nm.

2.6 | RNA collection and quantitative reverse transcription polymerase chain reaction

Cells were seeded in 6-well plates, and total RNA was extracted using TRIzol reagent (Invitrogen). RNA concentrations were detected with Nano Drop 8000 spectrophotometer (Pierce Thermo Scientific) and calculated from the absorbance at 260 nm, and purity was assessed by the 260:280 absorbance ratio. Then total RNA was reverse-transcribed into single-strand cDNA using a Prime Script RT Reagent Kit (Takara, Tokyo, Japan) based on the manufacturer's instructions. qRT-PCR reaction was performed using Power SYBR Green PCR Master Mix (Roche Applied Science, Mannheim, Germany) according to

the manufacturer's instructions. The expression of glyceraldehyde 3-phosphate dehydrogenase (*GAPDH/Gapdh*) was detected for normalization of gene expressions. The primers used for homo sapiens: *DUSP5*, *OSX*, *RUNX2*, and *GAPDH*; Mus musculus: *Dusp5*, *Osx*, *Runx2*, and *Gapdh* are listed in Table 1. $2^{\wedge-\Delta\Delta CT}$ method was used for analyzing gene expressions.

2.7 | Western blot

The total cellular protein was prepared in radioimmunoprecipitation assay (RIPA) buffer supplemented with 1% phosphatase inhibitor (Roche) and 2% protease inhibitor cocktail (Roche) on ice for 30 minutes. Then the lysates were centrifuged at 14000 rpm at 4°C for 20 minutes to collected supernatants. The protein concentrations were measured by using Pierce BCA protein assay kit (Thermo Fisher Scientific). Equal amount of the protein extracts was separated on proper dodecyl sulfate,sodium salt-polyacrylamide gel electrophoresis (SDS-PAGE) and transferred to polyvinylidene difluoride membrane (PVDF membrane, Millipore, Billerica, Massachusetts). After blocking in 5% milk for 1 hour, the membranes were incubated overnight at 4°C with the primary antibodies. After rinsed in Tris-buffered saline-Tween 20 (TBST) for 3 times, the membrane was incubated with IgG horseradish peroxidase-linked secondary antibody (1:10 000) for 1 hour. After another 3 rinses in TBST, the electrochemiluminescence kit (CWBIO) was used to detect the protein bands. The following antibodies were used: Cell Signaling Technology (Beverly, Massachusetts): RUNX2 (12556), phosphor-SMAD1/5/9 (13820), phosphor-SMAD1/5 (9516), phosphor-SMAD1 (5753), SMAD1 (6944), SMAD5 (12534), phosphor-SMAD2 (3108), phosphor-SMAD3 (9520), SMAD2/3 (8685), Myc (2276), GST (2622); Abcam (Cambridge, UK): DUSP5 (ab200708), SCP1 (ab175191), OSX (ab209484); Huaxingbochuang Biotechnology (Beijing, China): GAPDH (HX1832); sigma: Flag (SAB4200071), Proteintech: IgG (B900620), HRP-IgG Light Chain Specific (SA00001-7 L), HA-Tag (66006-1-Ig); Thermo Fisher (Waltham, Massachusetts): SCP2 (PA5-35984); Santa Cruz (Dallas, Texas): DUSP5 (sc-393 801). The protein levels were shown and quantified using ImageJ software (National Institutes of Health, Bethesda, Maryland).

2.8 | Coimmunoprecipitation

The total protein of transfected cells was extracted and quantified according to the same manufactures as that of Western blot. 30-60 micrograms protein per sample was prepared for input lane, and the rest lysis was divided equally into 2 parts, IgG group and experiment group, which were incubated with the primary antibodies at 4°C overnight. Then 40 μL protein A/G magnetic beads (HY-K0202, MCE, China) were added to incubate with the antibodies for another 1 to 2 hours. After five rinses by RIPA buffer mixture, the protein samples were denatured and eluted with 2 × SDS loading dye (P1018, Solarbio, China) at 99°C for 5 minutes. Next, all samples were loaded and analyzed using Western blot.

2.9 | Expression and purification of recombinant proteins

E coli BL21 (DE3) was used to express Glutathione S-transferase (GST) fusion proteins. The *Escherichia coli* cells with the GST and GST-DUSP5 plasmid were grown in luria broth media containing 100 μg/mL ampicillin at 37°C for approximate 12 hours with shaking. Then the expression of GST and GST-DUSP5 was induced by addition of 100 μM isopropyl β-D-1-thiogalactopyranoside (11020, Solarbio) overnight at 16°C with shaking. Next, 80 mL culture was spin down at 4000 rpm for 10 minutes and discard the supernatant. The bacterial pellet was dissolved in 1 mL of PBS (plus 1 mg/mL lysozyme, L6876, Sigma) with protease inhibitors for 15 minutes on the ice, followed by adding np-40 (final 0.5%, KEP705-100, Keygen, China) rotate at 4°C for 30 minutes. Then the lysates were centrifuged at 14 000 rpm, 4°C for 15 minutes to collected supernatants. 40 μL of 50% glutathione sepharose beads (C600031-0006, Sangon Biotech, China) were rocked with the supernatants at 4°C for 2 hours. After that, the beads were collected by centrifuging at 2000 rpm, 4°C for 1 minute and was washed with GST washing buffer (20 mM Tris, pH 7.4, Solarbio) containing 0.1 mM EDTA (E1170, Solarbio) and100 mM NaCl (10 019 318, Hushi, China) for 4 times. Then, the beads suspension was stored at 4°C for subsequent immunoprecipitation.

2.10 | GST pull-down

HEK293T cell lysate was prepared according to the Western blot procedures. Appropriate amount of protein was mixed with 1 × SDS loading dye (WB200, New Cell & Molecular Biotech, China), which served as the input sample. Then the above GST and GST-DUSP5 beads suspension was incubated with 1 mg protein respectively overnight at 4°C. After that, the reaction mixtures were washed 4 times with NETN buffer (0.5% np-40, 0.1 mM EDTA, 20 mM Tris pH 7.4, 300 mM NaCl). Finally, proteins were solubilized with 1 × SDS loading buffer and separated by SDS-PAGE, followed by determination with Western blot method.

2.11 | Bone formation in vivo

hMSCs infected with lentivirus (sh*DUSP*-1, sh*DUSP*-2, sh*DUSP*-3, or NC; vector or *DUSP5*; vector/sh*DUSP5* or *DUSP5*/sh*DUSP5*) were prepared prior to the in vivo transplantation. After being trypsinized and resuspended, the cells were incubated with beta-tricalcium phosphate (β-TCP; Bicon, Boston, Massachusetts) particles for 1 hour at 37°C, followed by centrifugation at 1000 rpm for 5 minutes, and then implanted into the subcutaneously dorsal space of 6-week-old BALB/c homozygous nude (nu/nu) mice (n = 8 per group). After 8 weeks, samples were harvested, fixed using 4% paraformaldehyde for 24 hours, and decalcified for 14 days in 10% EDTA (pH 7.4). Then

the samples were dehydrated and embedded in paraffin. Paraffin sections with 5 to 6 μm thickness were stained with hematoxylin and eosin (H&E). All in vivo studies were performed under the approval of the Institutional Animal Care and Use Committee of the Peking University Health Science Center (LA2019019), and were performed in accordance with the Institutional Animal Guidelines.

2.12 | Microcomputed tomagraphy and bone morphometric analysis

6-8-week-old female C57BL/6 mice were purchased from Charles River Corporation (Beijing, China) and randomly divided into 2 groups, OVX and SHAM group. Operation was bilaterally conducted under anaesthetization with pentobarbital sodium injection (50 mg/kg). After 12 weeks, the femurs were harvested and analyzed and mBMMSCs were obtained. For in vivo treatment assay, 12 weeks after surgery, OVX group was randomly divided into two subgroups and were injected vector or *Dusp5* lentivirus (titer: 1×10^8 TU/mL, 200 μL, for 1 time) through tail vein respectively. After 1 month, the femurs were harvested and analyzed. mBMMSCs were obtained and cultured in PM or OM, after then, ALP and ARS staining and quantification, qRT-PCR and Western blot assays were used to evaluate osteogenic differentiation potential of mBMMSCs. Conditions of three-dimensional images were an effective pixel size of 8.82 μm, voltage of 80 kV, tube current of 500 μA, and exposure time of 1500 ms in each of the 360 rotational steps. An Inveon Research Workplace (Siemens, Munich, Germany) software was used to quantification of the images, including bone volume/total volume (BV/TV), trabecular number (Tb. N), trabecular separation (Tb. Sp), trabecular thickness (Tb. Th), and bone mineral density (BMD). This study was approved by the Institutional Animal Care and Use Committee of the Peking University Health Science Center (LA2019019), and was performed in accordance with the Institutional Animal Guidelines.

2.13 | Statistical analysis

SPSS Statistics 20.0 software (IBM, Armonk, New York) was used for statistical analysis. Differences between two groups were conducted by Student's *t* test, and comparisons between more than two groups were performed by one-way analysis of variance followed by a Tukey's post-hoc test. All values in this study were presented as mean ± SD from three independent experiments assays per group. $P < .05$ was considered statistically significant (*$P < .05$; **$P < .01$; ***$P < .001$).

3 | RESULTS

3.1 | DUSP5 promotes osteogenic differentiation of hMSCs both in vitro and in vivo

To investigate the potential role of the phosphatase DUSP5 in osteogenic differentiation of hMSCs, we examined the expression of DUSP5 in OM cultured hMSCs (Figure S1A-D). Since DUSP5 was significantly induced, we next constructed *DUSP5* stable knockdown hMSCs to further definite the impact of DUSP5 on hMSCs fate determination. Three shRNA sequences targeting *DUSP5* were used to avoid off-target effects, and the lentiviral transduction efficiency was confirmed by fluorescent staining (Figure S1E), qRT-PCR (Figure S1F), and Western blot (Figure 1A,B). As shown in Figure 1C-F, ALP activity and mineralized matrix formation were significantly inhibited in *DUSP5* knockdown cells. In addition, *DUSP5*-deficient hMSCs also resulted decreased OSX and RUNX2 expressions after cultured in OM for 1 week (Figures 1G-I and S1G-L). In consistent with the in vitro findings, nude mice transplants experiment confirmed that β-TCP particles mixed with sh*DUSP5*/hMSCs led to less ectopic bonelike tissue formation compared with those mixed with control cells (Figure 1J). On the other hand, *DUSP5* overexpression enhanced ALP activity (Figure 2A,B), promoted the formation of mineralized nodules (Figure 2C,D), and contributed to upregulated mRNA and protein levels of OSX and RUNX2 (Figures 2E,F and S2A). Moreover, compared with the control cells, *DUSP5*-overexpressing hMSCs promoted more bone-like tissues formation in vivo (Figure 2G). To further confirm the significant role of DUSP5 during osteogenic differentiation, we established *DUSP5* rescue cells by transfected *DUSP5*-overexpressing lentivirus into sh*DUSP5*/hMSCs. As shown in Figures 2H-N and S2B-J, the decreased osteogenic potential caused by *DUSP5* knockdown was reversed in *DUSP5* rescue cells. Collectively, our data demonstrated that DUSP5 was required for osteogenic differentiation of hMSCs both *in vitro* and *in vivo*.

3.2 | DUSP5 promotes the osteoblastic differentiation of hMSCs by activating SMAD1 signaling

To explore the molecular mechanisms underlying the regulation of osteogenic differentiation by DUSP5, we examined the phosphorylation status of several key components associated with osteogenic differentiation of hMSCs. Surprisingly, we observed that the phosphorylation of SMAD1 was remarkably decreased in *DUSP5* knockdown cells (Figures 3A,B and S3F). Conversely, *DUSP5*-overexpression hMSCs showed increased phosphorylation levels of SMAD1 signaling key indicators (Figure 3C,D). To further confirm the effect of DUSP5 on SMAD1 signaling activation, we investigated protein levels of p-SMAD1/5/9, p-SMAD1/5, and p-SMAD1 in *DUSP5* rescue cells; Figures 3E,F and S3G clearly demonstrated that DUSP5 restored the phosphorylation levels of SMAD1 signaling key factors. Meanwhile, we also investigated the phosphorylation levels of SMAD2 and SMAD3, as observed in Figure S3A-E, the expressions of p-SMAD2 or p-SMAD3 were not affected by DUSP5. Therefore, DUSP5 mainly correlated with the activation of SMAD1 signaling but not with SMAD2/3 signaling in hMSCs

In order to verify whether DUSP5 regulated hMSCs osteogenic differentiation through SMAD1 pathway, we performed siRNA-mediated knockdown of *SMAD1* in *DUSP5*-overexpressing hMSCs.

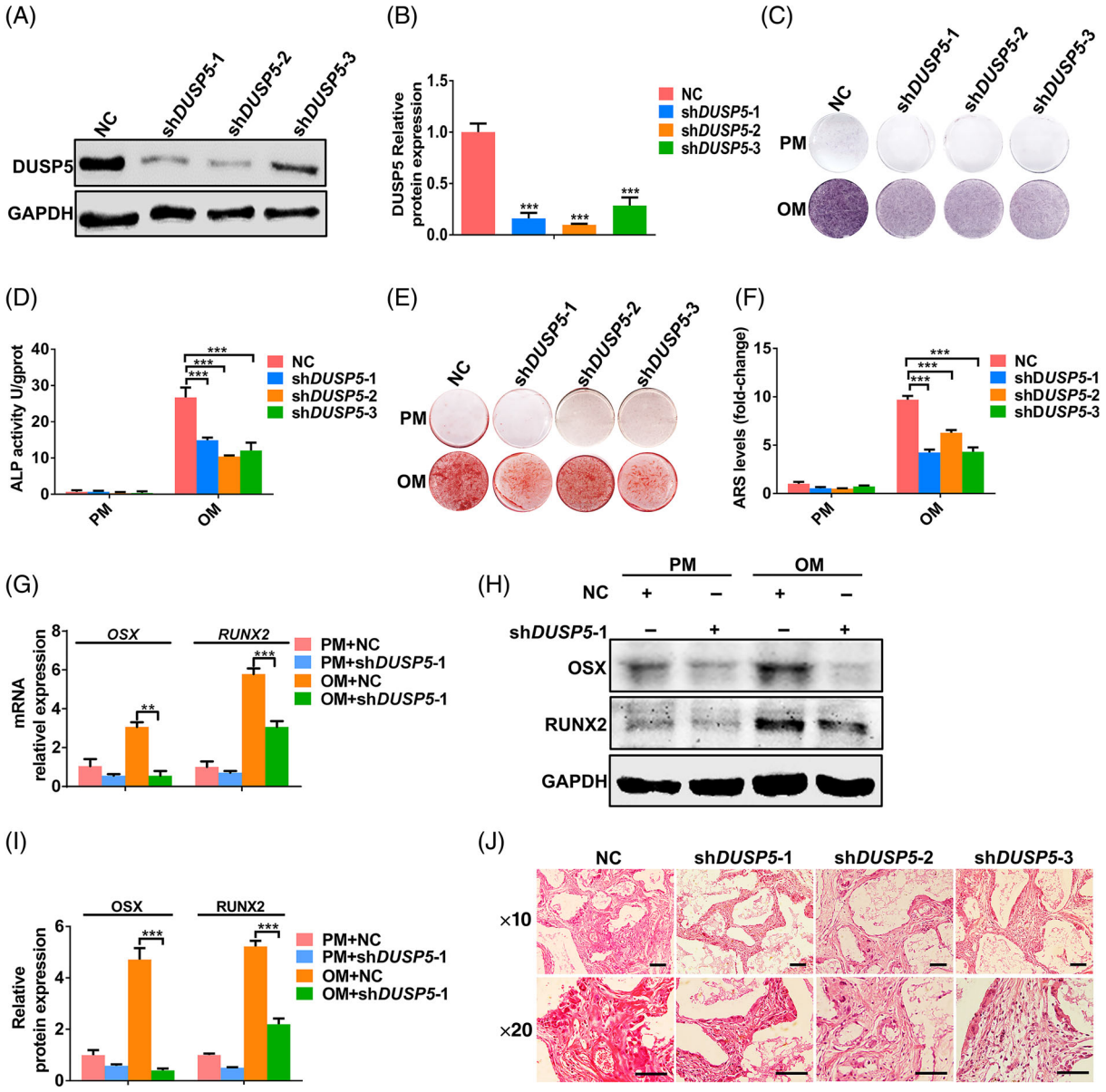

FIGURE 1 *DUSP5* deficiency inhibits osteogenic differentiation of hMSCs both in vitro and in vivo. A,B, Efficiency of *DUSP5* knockdown was validated by Western blot and protein quantitative analysis. GAPDH was used for normalization. C,D, ALP staining and quantification examination of NC and sh*DUSP5* hMSCs. E,F, ARS staining and quantification analysis of NC and sh*DUSP5* hMSCs. G, *OSX* and *RUNX2* mRNA relative expressions were examined by qRT-PCR in NC and sh*DUSP5*-1/hMSCs. *GAPDH* was used for normalization. H,I, OSX and RUNX2 protein expressions were determined by Western blot and protein quantitative analysis in NC and sh*DUSP5*-1/hMSCs. GAPDH was used for normalization. J, Ectopic bone formation capability of NC, sh*DUSP5*-1, sh*DUSP5*-2 and sh*DUSP5*-3 hMSCs in vivo was tested by H&E staining assay. Scale bar = 100 μm, n = 8. Data are represented as mean ± SD of three independent experiments. $^{**}P < .01$; $^{***}P < .001$, Student's *t* test and one-way ANOVA. ALP, alkaline phosphatase; ANOVA, analysis of variance; ARS, alizarin red S; DUSP5, dual-specificity phosphatase 5; GAPDH, glyceraldehyde 3-phosphate dehydrogenase; H&E, hematoxylin and eosin; hMSCs, human mesenchymal stem cells; NC, negative control for sh*DUSP5*-1, sh*DUSP5*-2, and sh*DUSP5*-3; OM, osteogenic medium; OSX, osterix; PM, proliferation medium; qRT-PCR, quantitative reverse transcription polymerase chain reaction; RUNX2, runt-related transcription factor 2

As shown in Figures 3G-J and S3H-K, we found that *SMAD1* deficiency could efficiently block the DUSP5-induced osteogenic potential as reflected by ALP activity, extracellular calcium nodular deposit, and the expressions of key osteogenic factors, such as OSX and RUNX2. Therefore, DUSP5 functioned as a positive regulator of hMSCs osteogenesis through modulating SMAD1 signaling activation.

3.3 | DUSP5 activates SMAD1 through a SCP1/2-dependent manner

As a phosphatase, why DUSP5 can facilitate instead of reducing the phosphorylation levels of SMAD1 signaling pathway? We next sought to determine whether DUSP5 regulated SMAD1 phosphorylation

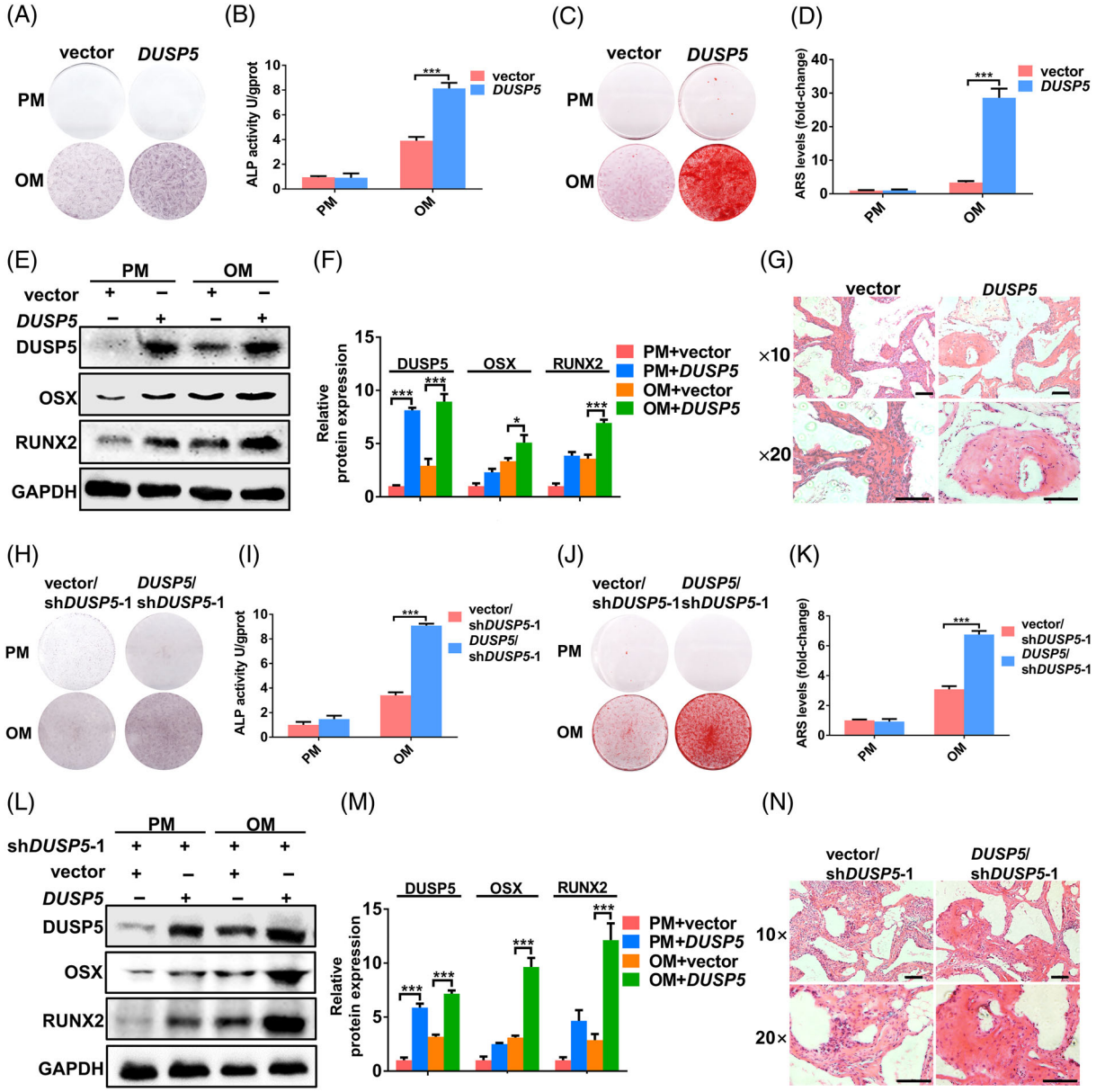

FIGURE 2 *DUSP5* overexpression promotes osteogenic differentiation of hMSCs both in vitro and in vivo. A-F, The osteogenic differentiation potential of vector and *DUSP5* hMSCs were detected by ALP staining and quantification examination (A, B), ARS staining and quantification examination (C, D), and Western blots of DUSP5, OSX, and RUNX2 protein expressions. GAPDH was used for normalization (E, F). G, H&E staining analysis of vector and *DUSP5* hMSCs in vivo. Scale bar = 100 μm, n = 8. H-M, *DUSP5*-1/hMSCs were rescued by transfecting with lentivirus expressing vector or *DUSP5*, and the capability of osteogenic differentiation was evaluated by ALP staining and quantification assay (H, I), ARS staining and quantification analysis (J, K), and Western blots of DUSP5, OSX, and RUNX2 protein levels (L, M) after osteogenic induction. GAPDH was used for normalization. N, H&E staining of ectopic bone formation of vector/sh*DUSP5*-1 and *DUSP5*/sh*DUSP5*-1 hMSCs in vivo. Scale bar = 100 μm, n = 8. Data are represented as mean ± SD of three independent experiments. **P* < .05; ****P* < .001, Student's *t* test and one-way ANOVA. ALP, alkaline phosphatase; ANOVA, analysis of variance; ARS, alizarin red S; DUSP5, dual-specificity phosphatase 5; GAPDH, glyceraldehyde 3-phosphate dehydrogenase; H&E, hematoxylin and eosin; hMSCs, human mesenchymal stem cells; OM, osteogenic medium; OSX, osterix; PM, proliferation medium; RUNX2, runt-related transcription factor 2; vector, negative control for *DUSP5*

indirectly through regulating the activity of kinases or phosphatases of SMAD1. Although we did not observe regulation of SMAD1 kinases by DUSP5, evident interaction of DUSP5 with SMAD1 phosphatases SCP1/2, but not with PPM1A, PP1, or PDP (Figure S4D-K) was discovered as determined by Co-IP experiments. First, Flag-DUSP5 and Myc-SCP1 plasmids were coexpressed in HEK293T cells. As shown in Figure S4A,B, immunoprecipitation of exogenous DUSP5 resulted in the coprecipitation of exogenous SCP1, and the converse precipitation also confirmed the interaction between the exogenous SCP1 and the exogenous DUSP5. Next, we transfected HEK293T cells with either Flag-DUSP5 or Myc-SCP1 alone, as shown in Figure 4A, exogenous DUSP5 bound to the endogenous SCP1, and

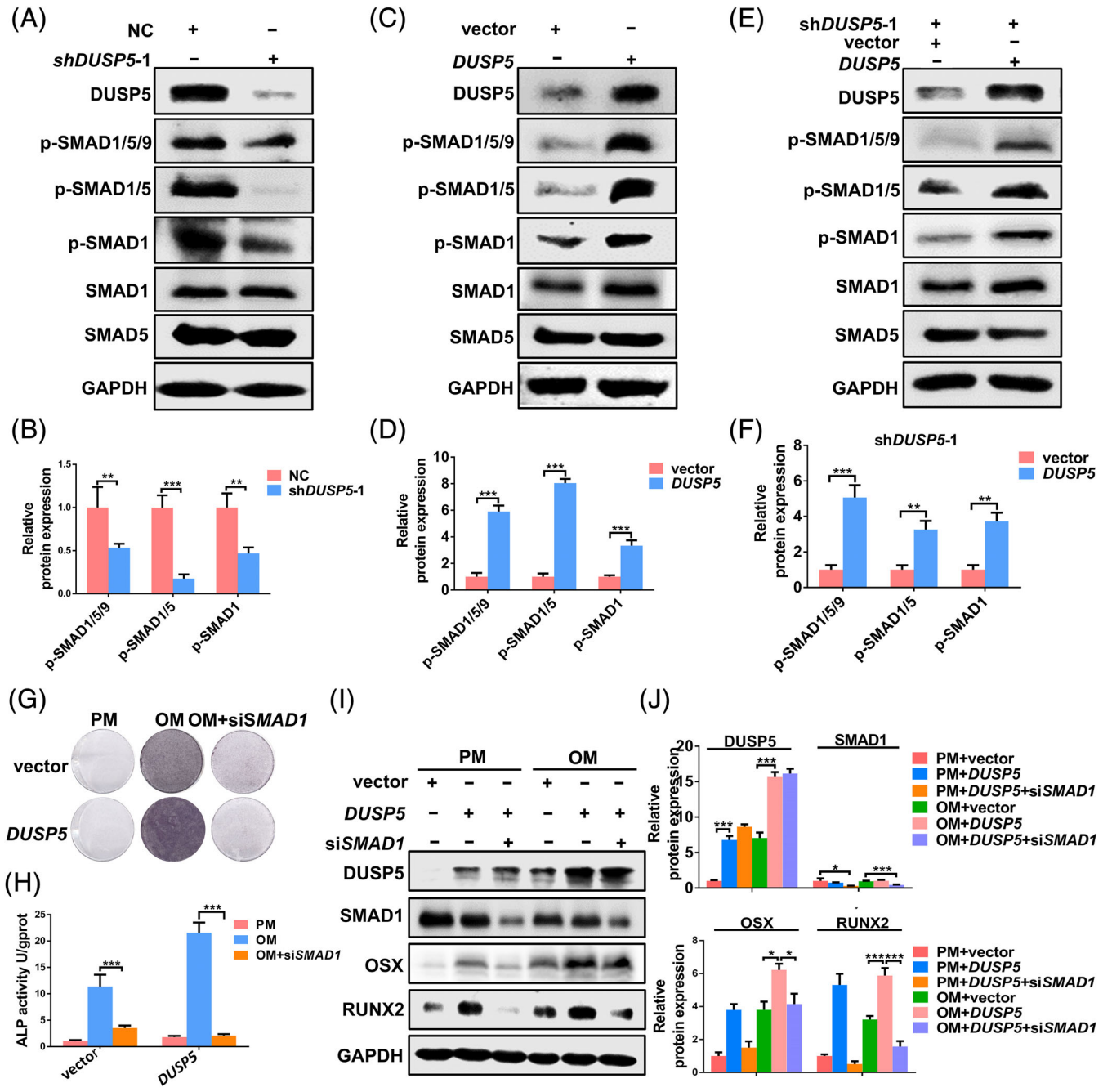

FIGURE 3 DUSP5 promotes the osteoblastic differentiation of hMSCs by activating SMAD1 signaling. A-F, p-SMAD1/5/9, p-SMAD1/5, and p-SMAD1 protein expressions were determined by Western blot and protein quantification analysis. SMAD1, SMAD5, and GAPDH were used for normalization. G,H, ALP staining and quantification assay. I,J, DUSP5, SAMD1, OSX, and RUNX2 protein expressions were determined by Western blot analysis. GAPDH were used for normalization. Data are represented as mean ± SD of three independent experiments. *$P < .05$, **$P < .01$, ***$P < .001$, Student's *t* test and one-way ANOVA. ALP, alkaline phosphatase; ANOVA, analysis of variance; DUSP5, dual-specificity phosphatase 5; GAPDH, glyceraldehyde 3-phosphate dehydrogenase; hMSCs, human mesenchymal stem cells; NC, negative control for sh*DUSP5*-1; OM, osteogenic medium; OSX, osterix; PM, proliferation medium; RUNX2, runt-related transcription factor 2; vector, negative control for *DUSP5*

equivalently, endogenous DUSP5 could also be detected in exogenous SCP1 immunoprecipitate (Figure 4B). Moreover, endogenous interaction between DUSP5 and SCP1 was confirmed in Figure 4C. Additionally, we examined their direct interaction by performing GST pull-down assay. As shown in Figure S4L, GST and GST-DUSP5 proteins were purified, and SCP1 could be pulled down with GST-DUSP5 (Figure 4D), reflecting that SCP1 bound DUSP5 directly. Similar experiments were performed to confirm the interaction between DUSP5 and SCP2, and as shown in Figures 4E-J and S4C, the interaction between DUSP5 and SCP2 also existed. All these data confirmed the presence of DUSP5/SCP1/2 complex.

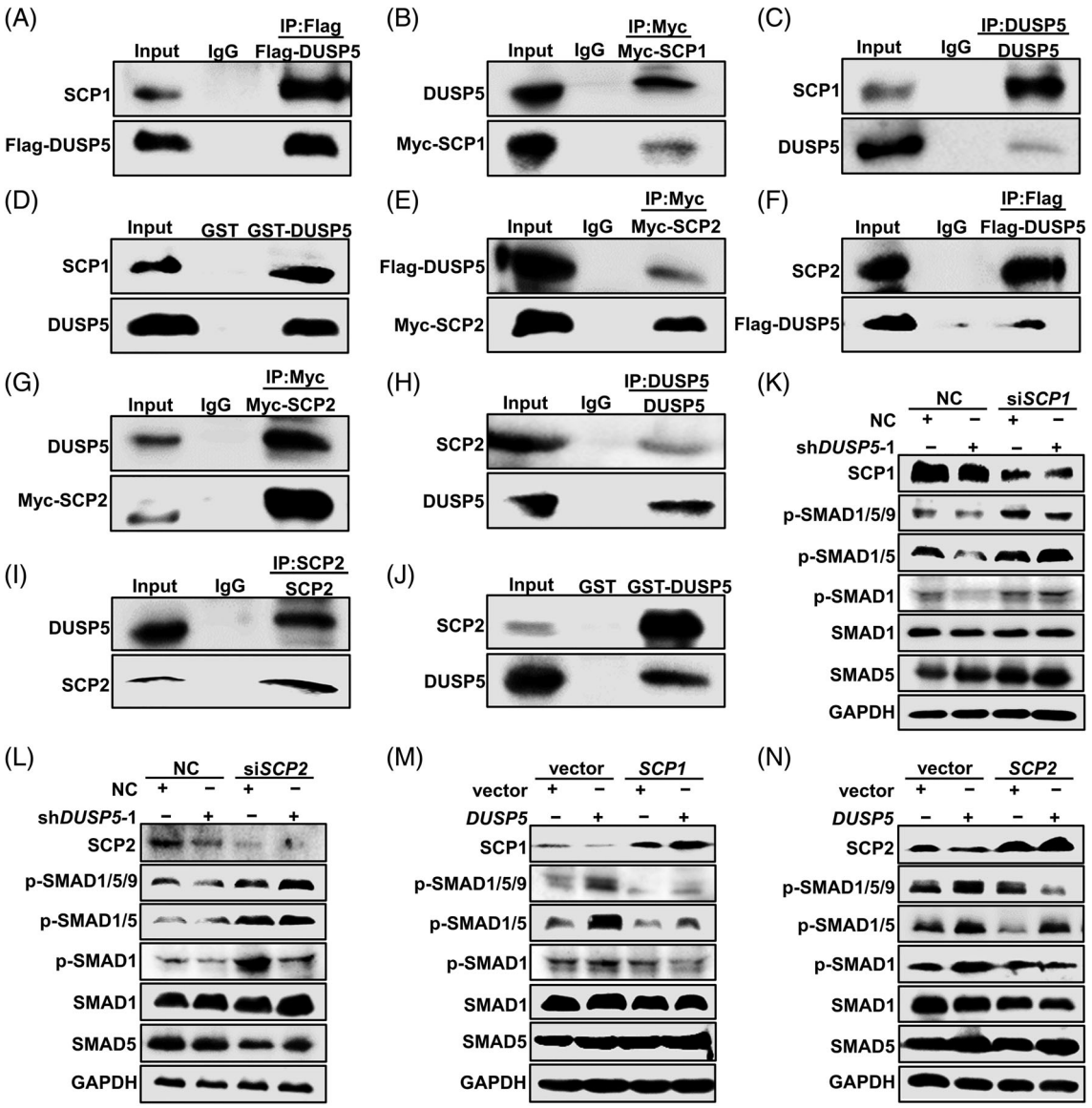

FIGURE 4 DUSP5 activates SMAD1 through a SCP1/2-dependent manner. A-C, Co-IP assay indicated the interaction between DUSP5 and SCP1. D, The combination of DUSP5 with SCP1 was confirmed by GST pull-down experiment. E-I, Co-IP assay showed the interaction between DUSP5 and SCP2. J, GST pull-down experiment validated that DUSP5 bound to SCP2. K-N, Western blots of protein levels of p-SMAD1/5/9, p-SMAD1/5, and p-SMAD1. SMAD1, SMAD5, and GAPDH were used for normalization. Data represented were repeated three times. Co-IP, coimmunoprecipitation; DUSP5, dual-specificity phosphatase 5; GAPDH, glyceraldehyde 3-phosphate dehydrogenase; GST, glutathione S-transferase; NC, negative control for sh*DUSP5*-1; SCP1, small C-terminal phosphatase 1; SCP2, small C-terminal phosphatase 2; vector, negative control for *DUSP5* or *SCP1/2*

To further explore whether the effect of DUSP5 on SMAD1 phosphorylation was dependent on SCP1/2, we silenced or overexpressed *SCP1/2* in hMSCs, and the protein levels of p-SMAD1/5/9, p-SMAD1/5, and p-SMAD1 were tested by Western blot, as shown in Figure S5A,B, *SCP1/2* deficiency led to greater phosphorylation levels, whereas upregulation of *SCP1/2* by plasmids transfection inhibited the induction of p-SMAD1/5/9, p-SMAD1/5, and p-SMAD1 (Figure S5C,D), indicating that SCP1/2 act as phosphatases of SMAD1 in hMSCs. Subsequently, we examined the expressions of p-SMAD1/5/9, p-SMAD1/5, and p-SMAD1 after siRNA-mediated suppression of *SCP1/2* in sh*DUSP5*/hMSCs. As shown in Figures 4K,L and S5E,F, the downregulated phosphorylation levels resulted from *DUSP5*-deficiency were rescued by *SCP1/2* depletion. Consistently, overexpression SCP1/2 inhibited the effect of DUSP5 on the SMAD1 phosphorylation (Figure 4M,N). These results confirmed that the activation of SMAD1 signaling by DUSP5 was dependent on SCP1/2.

3.4 | The linker region of DUSP5 interacts with the phosphatase domain of SCP1/2

Structurally, DUSP5 is composed of three domains: substrate-binding domain (SBD, 1-140aa), a linker region (LR, 141-178aa), and a phosphatase domain (PD, 179-384aa). While SCP1 contains a central

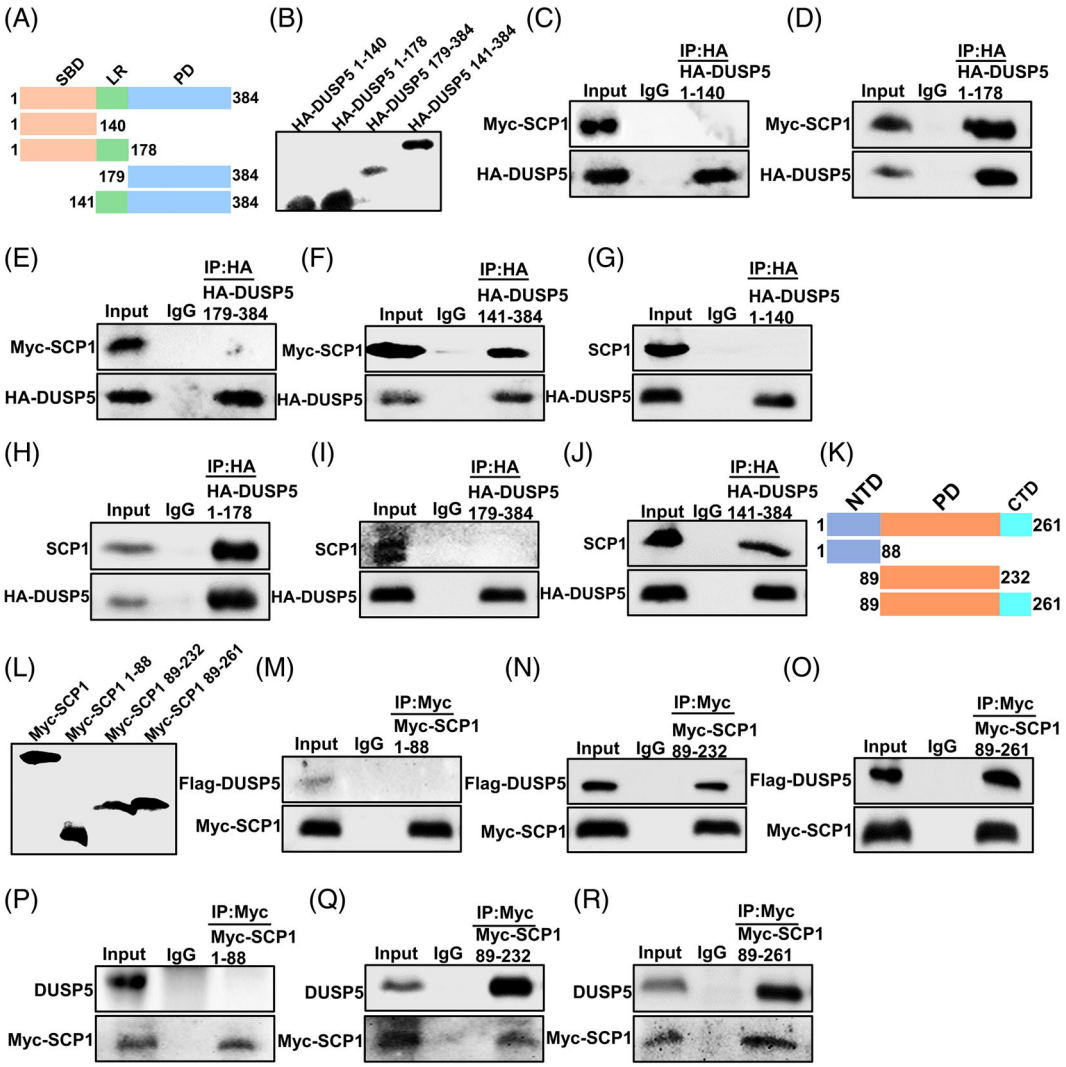

FIGURE 5 The linker region of DUSP5 interacts with the phosphatase domain of SCP1/2. A, Schematic representation of DUSP5 fragments. B, DUSP5 fragments were determined by Western blot. C-J, Co-IP assays of the interaction between DUSP5 fragments and SCP1. K, Schematic representation of SCP1 fragments. L, Full-length and segments of SCP1 were determined by Western blot. M-R, The combination between SCP1 fragments and DUSP5 was confirmed by Co-IP experiment. Data represented were repeated three times. Co-IP, coimmunoprecipitation; CTD, C-terminal domain; DUSP5, dual-specificity phosphatase 5; LR, linker region; NTD, N-terminal domain; PD, phosphatase domain; SBD, substrate-binding domain; SCP1, small C-terminal phosphatase 1

phosphatase domain (PD, 89-232aa), a short N-terminal (NTD, 1-88aa) and CTD (233-261aa). To determine the specific functional domains of DUSP5 and SCP1 for their interaction, we generated a series of segments, including HA-tagged SBD (1-140), SBD + LR (1-178), PD (179-384) and LR + PD (141-384) of DUSP5 and Myc-tagged N-terminal domain (NTD, 1-88), PD (89-232) and PD + CTD (89-261) of SCP1. Schematic representations of DUSP5 and SCP1 fragments involved are shown in Figures 5A,K, and their molecular mass was determined with HA or Myc antibodies respectively by Western blot (Figure 5B,L). Then, different HA-DUSP5 fragments were coexpressed with Myc-SCP1 in HEK293T cells. As shown in Figure 5C-F, Myc-SCP1 interacted with 1 to 178 and 141 to 384 fragments (both containing the linker region), but not with the SBD or PD region of DUSP5. Similarly, endogenous SCP1 bound primarily to HA-DUSP5 fragments possessing the linker region (Figure 5G-J). Previous research has testified that the PD of SCPs is essential for its activity to terminate SMAD signal, so it was great interest to explore whether the PD of SCP1 mediated the interaction between DUSP5 and SCP1. As shown in Figure 5M-R, exogenously expressed SCP1 fragments containing PD (89-232 and 89-261 fragments) obviously combined with both exogenous and endogenous DUSP5, while N-terminal fragment failed to interact with DUSP5. Our data demonstrated that the linker region of DUSP5 and the PD of SCP1 were indispensable for their interaction. Since SCP2 shares the sufficient homology with SCP1, here the interaction of SCP2 fragments with DUSP5 was not shown.

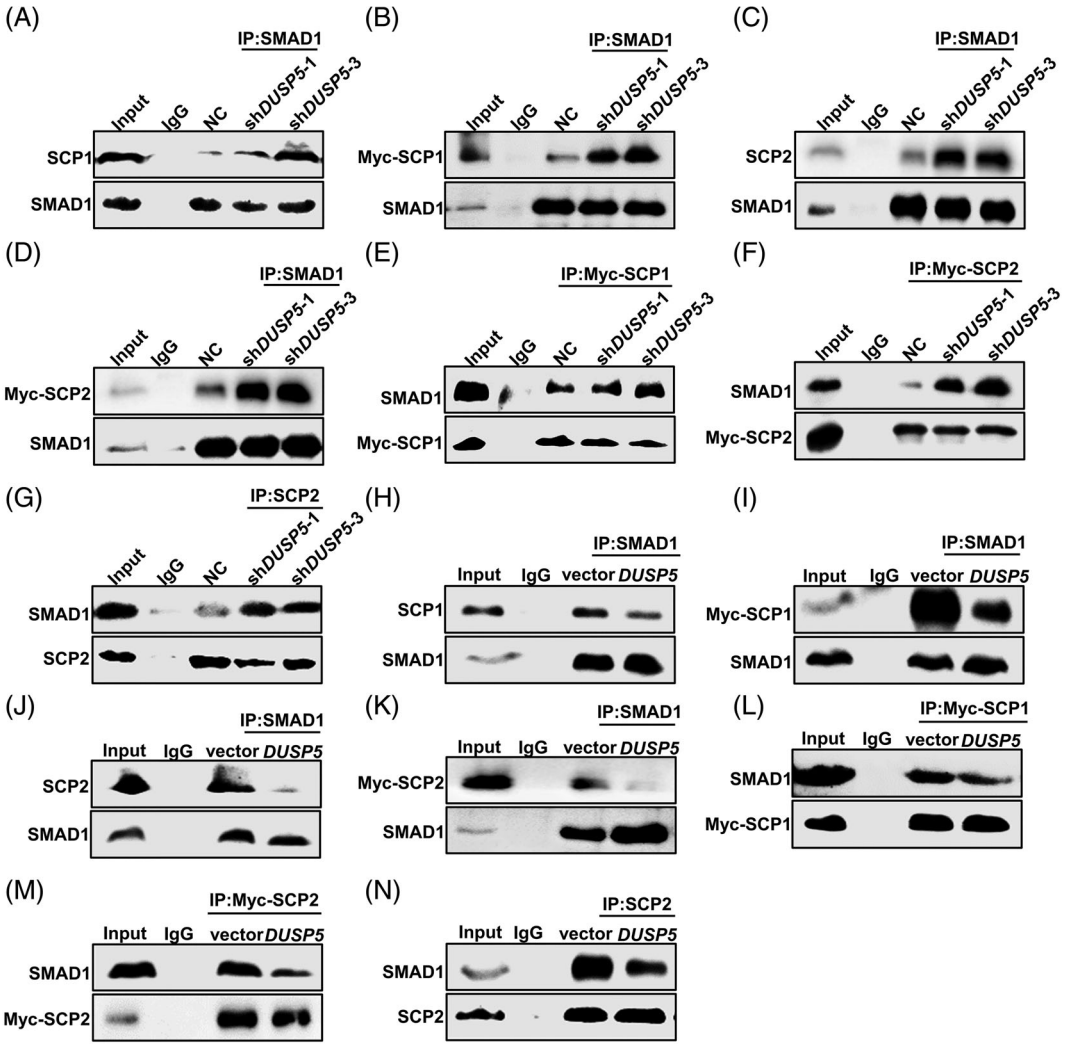

FIGURE 6 Competitive combination of DUSP5 and SCP1/2 with SMAD1. A-G, Co-IP assay was performed to determine the interaction between SCP1 and SMAD1, and the interaction between SCP2 and SMAD1 in NC, sh*DUSP5*-1 and sh*DUSP5*-3 HEK293T cells. H-N, The interaction between SCP1 and SMAD1, and the interaction between SCP2 and SMAD1 in vector and *DUSP5* HEK293T cells was detected by Co-IP experiment. Data represented were repeated three times. Co-IP, coimmunoprecipitation; DUSP5, dual-specificity phosphatase 5; NC, negative control for sh*DUSP5*-1 and sh*DUSP5*-3; SCP1, small C-terminal phosphatase 1; SCP2, small C-terminal phosphatase 2; vector, negative control for *DUSP5*

3.5 | Competitive combination of DUSP5 and SCP1/2 with SMAD1

To explore how dose DUSP5 promote the phosphorylation of SMAD1 through SCP1/2, we first confirmed the interaction between SCP1/2 and SMAD1 (Figure S6A,B), which consistent with previous studies.[16,44] Moreover, we detected that DUSP5 physically interacted with SMAD1 but not with SMAD4 (Figure S6C-H). We next examined whether DUSP5 expression level influenced SCP1/2-SMAD1 interaction. To this end, we investigated the ability of SMAD1 and SCP1/2 to coprecipitate with each other after silencing or increasing *DUSP5* expression. As shown in Figure 6A-D, precipitation of SMAD1 resulted in coprecipitation of SCP1/2 including both endogenous and exogenous forms, which was augmented by silenced expression of *DUSP5*. Similarly, coprecipitated SMAD1 by ectopically expressed SCP1/2 and endogenous SCP1/2 was also increased in *DUSP5*-deletion cells compared with that in NC cells (Figure 6E-G). In addition, *DUSP5* overexpression significantly attenuated the association of SMAD1 with SCP1/2 (Figure 6H-N). Altogether, our finding suggested that DUSP5 intervened the combination of SCP1/2 with SMAD1, which was responsible for SMAD1 dephosphorylation, and resulted in the activation of SMAD1 signaling.

3.6 | DUSP5 is a potential target for osteoporosis treatment

Since DUSP5 promoted hMSCs osteogenic differentiation significantly, we next intended to explore the role of DUSP5 in bone metabolism. OVX or SHAM operation was performed and the mice were

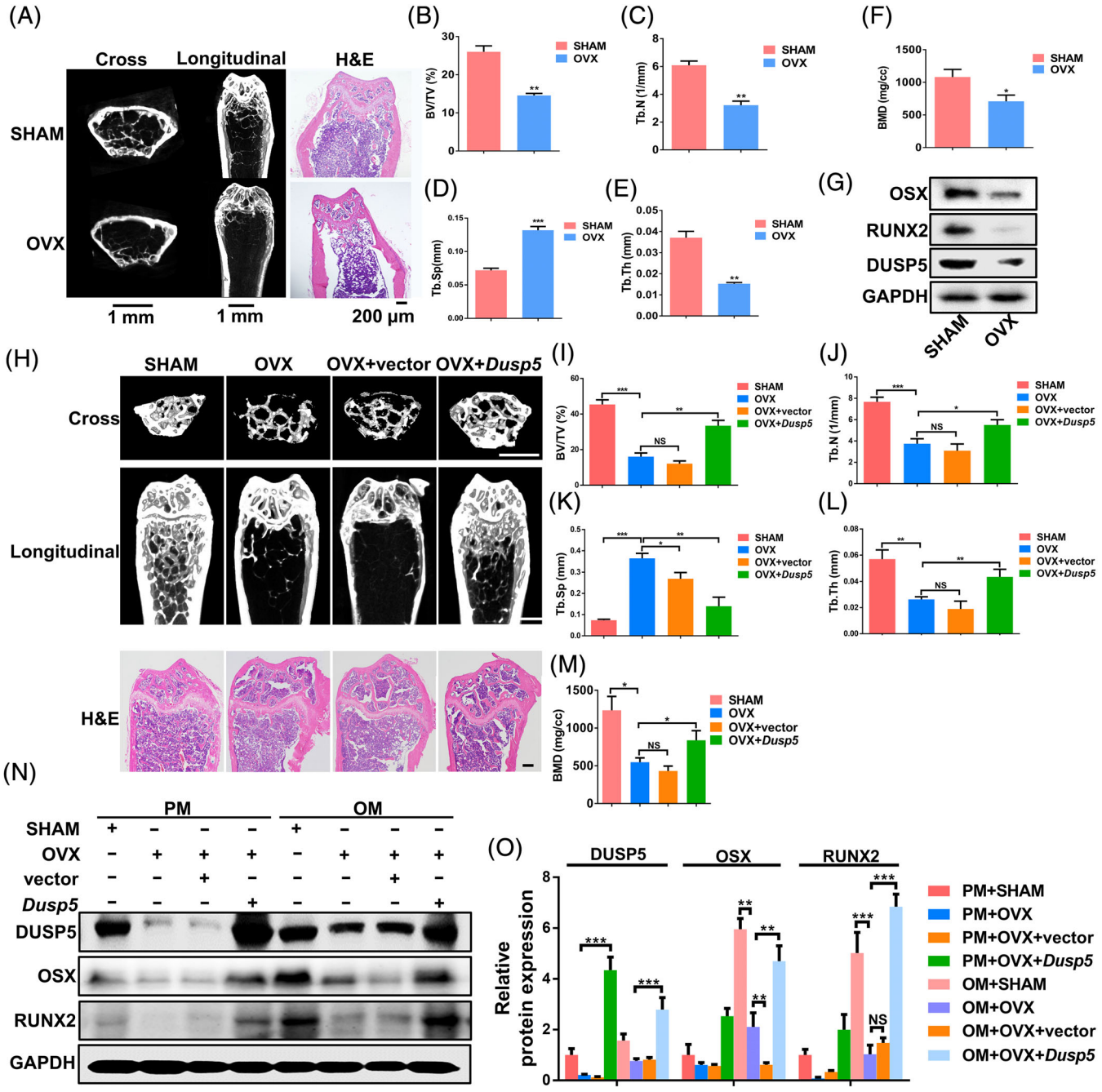

FIGURE 7 DUSP5 is a potential target for osteoporosis treatment. A, Micro-CT and H&E staining results of femur metaphysis of SHAM and OVX mice. Scale bar for cross and longitudinal images of micro-CT = 1 mm; Scale bar for H&E sections = 200 μm. B-F, Quantitative measurements of BV/TV, Tb.N, Tb.Sp, Tb.Th, and BMD of SHAM and OVX groups. G, Western blots of OSX, RUNX2, and DUSP5 protein expressions in SHAM and OVX mBMMSCs. GAPDH was used for normalization. H-M, Femur metaphysis bone mass analysis of SHAM, OVX, OVX + vector, and OVX + *Dusp5* mice was conducted by micro-CT, H&E staining (H), and quantitative measurements (I-M). Scale bar for cross and longitudinal images of micro-CT = 1 mm; Scale bar for H&E sections = 200 μm. N,O, Western blots of DUSP5, OSX, and RUNX2 protein expressions of SHAM, OVX, OVX + vector, and OVX + *Dusp5* mBMMSCs. GAPDH was used for normalization. Data are represented as mean ± SD of three independent experiments. NS: $P > .05$, $^{*}P < .05$, $^{**}P < .01$, $^{***}P < .001$, Student's *t* test and one-way ANOVA. ANOVA, analysis of variance; BMD, bone mineral density; BV/TV, bone volume/tissue volume; DUSP5, dual-specificity phosphatase 5; GAPDH, glyceraldehyde 3-phosphate dehydrogenase; H&E, hematoxylin and eosin; mBMMSCs, mouse bone marrow-derived mesenchymal stromal cells; micro-CT, micro-computed tomography; OM, osteogenic medium; OSX, osterix; OVX, ovariectomized; PM, proliferation medium; RUNX2, runt-related transcription factor 2; SHAM, negative control for OVX; Tb.N, trabecular number; Tb.Sp, trabecular spacing; Tb.Th, trabecular thickness; vector, negative control for *Dusp5*

sacrificed at 3 months, both micro-CT and H&E staining of mice femur metaphysis proved that OVX group presented obvious bone loss compared with SHAM group (Figure 7A), which further confirmed by quantitative measurements of BV/TV, Tb.N, Tb.Sp, Tb.Th, and BMD (Figure 7B-F). Meanwhile, mBMMSCs were flushed; qRT-PCR and Western blot analysis indicated that DUSP5 mRNA and protein expressions were evidently downregulated accompanied by decreased OSX and RUNX2 in mBMMSCs from OVX mice (Figures 7G and S6I,J), suggesting that DUSP5 might play a predominant role in bone homeostasis. Subsequently, to determine the therapeutic effect of DUSP5 on osteoporosis, we injected mouse *Dusp5* or vector lentivirus into OVX mice through tail vein. As expected, although there was no significant difference of bone histomorphometry measurements between OVX + vector and OVX groups, *Dusp5* lentivirus injection alleviated osteoporosis remarkably, as detected by micro-CT analysis and H&E staining (Figure 7H-M). Consistently, mBMMSCs from OVX + *Dusp5* mice had greater osteogenic potential compared with that of OVX mice, reflected by higher ALP activity, more extracellular calcium deposit, and higher OSX and RUNX2 mRNA and protein expressions levels (Figures 7N,O and S6K-O). Therefore, our data suggested a promising therapeutic potential of DUSP5 in osteoporosis.

4 | DISCUSSION

DUSP5, potentially hydrolyzing the phosphoryl group from serine/threonine and tyrosine residues of ERK1/2,[41] has been extensively characterized as a modulator under various physiological and pathological circumstances such as tumorigenesis and immune disorders.[45-48] In the current study, we discover a new role of DUSP5 as a positive regulator in MSCs osteogenic differentiation both *in vitro* and *in vivo*. Interestingly, DUSP5 exerts osteogenic function by activating SMAD1 signaling pathway instead of dephosphorylating its substrates, extending the regulatory mechanisms of DUSP5 and ascertaining the notion that each step in SMAD1 signaling is fine-tuned by modulation and crosstalk with other signaling pathways or factors to achieve specific cell differentiations.[49,50] However, the functional validation of DUSP5 in osteogenesis may be more faithfully recapitulated by expediting the construction of knockout animal models.

As a phosphatase, DUSP5 induces the phosphorylation of SMAD1 signaling key factors, arousing our interest to explore the underlying mechanisms. It is known that SMAD1 phosphatases in nucleus weaken signal transduction to the required level through protein dephosphorylation.[51] For instance, SCP1-3 decrease the extent and duration of SMAD1 phosphorylation at C-terminal tail and the linker region in response to BMP and attenuate the strength of endogenous BMP gene responses.[11,12] PP2A Cα and PPM1A play negative roles in osteoblast differentiation through the dephosphorylation of SMAD1/5/9.[9,52,53] Surprisingly, we observe the significant interaction between DUSP5 and SMAD1 phosphatases SCP1/2, and verify that DUSP5 promotes SMAD1 activation in a SCP1/2-dependent manner. The association of DUSP5 with SCP1/2 might impair the SCP1/2-SMAD1 complex, which is further illustrated by DUSP5 competitively inhibiting the SCP1/2-SMAD1 combination. Therefore, the positive effect of DUSP5 on SMAD1 signaling is dependent upon the relief of upstream phosphatases SCP1/2 inhibition. It is prevalently believed that the phosphatase domains take primary responsibility for the catalytic mechanisms of phosphatases. For example, PP2C-type phosphatase core domain contributes to the formation of a surface substrate-binding groove, and is essential for the selectivity of Photosystem II (PSII) core phosphatase (PBCP) toward PSII proteins.[54] Nevertheless, there are also exceptions. In *Drosophila*, for instance, the N-terminal prion-like domain of Hzg orchestrates its phosphatase activity and controls embryonic development.[55] We validate the linker region of DUSP5 mainly acts on the biological effect during osteogenesis process, providing an example of the linker region that allows DUSP5 to gain crucial functionality and might be a potential target.

Deregulation of protein phosphorylation has been implicated in various diseases including osteoblast dysfunctions, and emerging therapeutic strategies focused on the drugs design targeting kinases and phosphatases are effective to modulate the biological actions. Tremendous efforts spared in kinase-targeted drugs have also invigorated discussions regarding phosphatases.[56-59] DUSPs are believed a desirable target for medical research for their small size and simple domain structure. Beyond that, due to the compensatory effects among different DUSPs, pharmacological functions are likely to be safer, milder, and fewer side effects.[17] As such, strategies designed to upregulate DUSP5 expression in cells could be beneficial for treating disabilities manifested by osteogenic dysfunction. We show in this report that the administration of *Dusp5* lentivirus via tail intravenous injection obviously attenuates bone loss in OVX mice, which confirms the possible therapeutic potential of DUSP5. It is noteworthy that the linker region of DUSP5 plays an essential role in MSCs osteogenesis, probably providing a theoretical basis for design of small molecular compound specifically targeting this functional region.

5 | CONCLUSIONS

In conclusion, our study supplements a previously unknown role for DUSP5 that promotes MSCs osteoblastic differentiation by activating SMAD1 signaling pathway. Precisely, the linker region of DUSP5 interacts with the phosphatase domain of SCP1/2 and DUSP5 competitively inhibits SCP1/2-SMAD1 association, perturbating the dephosphorylation effect of SCP1/2 on SMAD1. Moreover, the findings that DUSP5 alleviates osteoporosis in mice strengthen the case for the therapeutic potential of DUSP5 in treating bone destruction diseases whose pathogenesis is thought to involve decreased MSCs osteogenic capability.

ACKNOWLEDGMENT

This work was supported by the National Natural Science Foundation of China under Grant 81970911 and 81870742, the Beijing Natural Science Foundation under Grant 7202233, and the Capital Culturing

Project for Leading Talents in Scientific and Technological, Innovation in Beijing under Grant Z171100001117169.

CONFLICT OF INTEREST

The authors declared no potential conflicts of interest.

AUTHOR CONTRIBUTIONS

Y.Z., P.Z.: conception and design, financial support, manuscript editing and final approval of manuscript, revised the manuscript; Xuejiao Liu: laboratory work, data collection and analysis, manuscript writing, revised the manuscript; Xuenan Liu and Yangge Du: experimental techniques; M.H., Y.T., Z.L., L.L., X.Z., Y.L.: data collection and final approval of manuscript, revised the manuscript; All authors agreed to be accountable for all aspects of the work.

DATA AVAILABILITY STATEMENT

The data that support the findings of this study are available from the corresponding author upon reasonable request.

ORCID

Xuejiao Liu https://orcid.org/0000-0002-2713-5779
Zheng Li https://orcid.org/0000-0003-0215-4401

REFERENCES

1. Xiao F, Qiu H, Cui H, et al. MicroRNA-885-3p inhibits the growth of HT-29 colon cancer cell xenografts by disrupting angiogenesis via targeting BMPR1A and blocking BMP/Smad/Id1 signaling. *Oncogene*. 2015;34:1968-1978.
2. Salazar V, Gamer L, Rosen V. BMP signalling in skeletal development, disease and repair. *Nat Rev Endocrinol*. 2016;12:203-221.
3. Parrow N, Gardenghi S, Ramos P, et al. Decreased hepcidin expression in murine β-thalassemia is associated with suppression of Bmp/-Smad signaling. *Blood*. 2012;119:3187-3189.
4. Shi Y, Massagué J. Mechanisms of TGF-beta signaling from cell membrane to the nucleus. *Cell*. 2003;113:685-700.
5. Rahman M, Akhtar N, Jamil H, et al. TGF-β/BMP signaling and other molecular events: regulation of osteoblastogenesis and bone formation. *Bone Res*. 2015;3:15005.
6. Wu M, Chen G, Li Y. TGF-β and BMP signaling in osteoblast, skeletal development, and bone formation, homeostasis and disease. *Bone Res*. 2016;4:16009.
7. Kushioka J, Kaito T, Okada R, et al. A novel negative regulatory mechanism of Smurf2 in BMP/Smad signaling in bone. *Bone Res*. 2020;8:41.
8. Duan X, Liang YY, Feng XH, Lin X. Protein serine/threonine phosphatase PPM1A dephosphorylates Smad1 in the bone morphogenetic protein signaling pathway. *J Biol Chem*. 2006;281:36526-36532.
9. Lin X, Duan X, Liang Y, et al. PPM1A functions as a Smad phosphatase to terminate TGFβ signaling. *Cell*. 2016;125:915-928.
10. Hong BC, Shen J, Ip YT, et al. Identification of phosphatases for Smad in the BMP/DPP pathway. *Genes Dev*. 2006;20:648-653.
11. Sapkota G, Knockaert M, Alarcón C, Montalvo E, Brivanlou AH, Massagué J. Dephosphorylation of the linker regions of Smad1 and Smad2/3 by small C-terminal domain phosphatases has distinct outcomes for bone morphogenetic protein and transforming growth factor-beta pathways. *J Biol Chem*. 2006;281:40412-40419.
12. Knockaert M, Sapkota G, Alarcón C, et al. Unique players in the BMP pathway: small C-terminal domain phosphatases dephosphorylate Smad1 to attenuate BMP signaling. *Proc Natl Acad Sci USA*. 2006;103:11940-11945.
13. Shi Y. Serine/threonine phosphatases: mechanism through structure. *Cell*. 2009;139:468-484.
14. Zhang Y, Kim Y, Genoud N, et al. Determinants for dephosphorylation of the RNA polymerase II C-terminal domain by Scp1. *Mol Cell*. 2006;24:759-770.
15. Zhao Y, Xiao M, Sun B, et al. C-terminal domain (CTD) small phosphatase-like 2 modulates the canonical bone morphogenetic protein (BMP) signaling and mesenchymal differentiation via Smad dephosphorylation. *J Biol Chem*. 2014;289:26441-26450.
16. Goto K, Tong K, Ikura J, et al. HLA-B-associated transcript 3 (Bat3/Scythe) negatively regulates Smad phosphorylation in BMP signaling. *Cell Death Dis*. 2011;2:e236.
17. Huang C, Tan T. DUSPs, to MAP kinases and beyond. *Cell Biosci*. 2012;2(1):24.
18. Ríos P, Nunes-Xavier CE, Tabernero L, Köhn M, Pulido R. Dual-specificity phosphatases as molecular targets for inhibition in human disease. *Antioxid Redox Signal*. 2014;20:2251-2273.
19. Hao P, Li H, Lee M, et al. Disruption of a regulatory loop between DUSP1 and p53 contributes to hepatocellular carcinoma development and progression. *J Hepatol*. 2015;62:1278-1286.
20. Jimenez T, Barrios A, Tucker A, et al. DUSP9-mediated reduction of pERK1/2 supports cancer stem cell-like traits and promotes triple negative breast cancer. *Am J Cancer Res*. 2020;10:3487-3506.
21. Ramkissoon A, Chaney K, Milewski D, et al. Targeted inhibition of the dual specificity phosphatases DUSP1 and DUSP6 suppress MPNST growth via JNK. *Clin Cancer Res*. 2019;25:4117-4127.
22. Guo F, Zhang C, Wang F, et al. Deubiquitinating enzyme USP33 restrains docetaxel-induced apoptosis via stabilising the phosphatase DUSP1 in prostate cancer. *Cell Death Differ*. 2020;27:1938-1951.
23. Ding J, Li J, Wang H, et al. Long noncoding RNA CRNDE promotes colorectal cancer cell proliferation via epigenetically silencing DUSP5/CDKN1A expression. *Cell Death Dis*. 2017;8:e2997.
24. Yan X, Liu L, Li H, et al. Dual specificity phosphatase 5 is a novel prognostic indicator for patients with advanced colorectal cancer. *Am J Cancer Res*. 2016;6:2323-2333.
25. Ma Z, Gao X, Shuai Y, et al. EGR1-mediated linc01503 promotes cell cycle progression and tumorigenesis in gastric cancer. *Cell Prolif*. 2021;54:e12922.
26. Ueda K, Arakawa H, Nakamura Y. Dual-specificity phosphatase 5 (DUSP5) as a direct transcriptional target of tumor suppressor p53. *Oncogene*. 2003;22:5586-5591.
27. Emanuelli B, Eberle D, Suzuki R, Kahn CR. Overexpression of the dual-specificity phosphatase MKP-4/DUSP-9 protects against stress-induced insulin resistance. *Proc Natl Acad Sci USA*. 2008;105:3545-3550.
28. Ge Y, Wang J, Wu D, et al. lncRNA NR_038323 suppresses renal fibrosis in diabetic nephropathy by targeting the miR-324-3p/DUSP1 axis. *Mol Ther Nucleic Acids*. 2019;17:741-753.
29. Pulido R, Aurtenetxe O, Zaldumbide L, et al. Neuroblastoma PTPome analysis unveils association of DUSP5 and PTPN1 expression with poor prognosis. *Ann Oncol*. 2017;28(suppl 7):vii21.
30. Triñanes J, Ten Dijke P, Groen N, et al. Tacrolimus-induced BMP/-SMAD signaling associates with metabolic stress-activated FOXO1 to trigger β-cell failure. *Diabetes*. 2020;69:193-204.
31. Ferguson B, Harrison B, Jeong M, et al. Signal-dependent repression of DUSP5 by class I HDACs controls nuclear ERK activity and cardiomyocyte hypertrophy. *Proc Natl Acad Sci USA*. 2013;110:9806-9811.
32. Halle M, Gabrielsen A, Paulsson-Berne G, et al. Sustained inflammation due to nuclear factor-kappa B activation in irradiated human arteries. *J Am Coll Cardiol*. 2010;55:1227-1236.
33. Pramanik K, Chun C, Garnaas M, et al. Dusp-5 and Snrk-1 coordinately function during vascular development and disease. *Blood*. 2009;113:1184-1191.

34. Lu D, Liu L, Ji X, et al. The phosphatase DUSP2 controls the activity of the transcription activator STAT3 and regulates TH17 differentiation. *Nat Immunol*. 2015;16(12):1263-1273.
35. Lu D, Liu L, Sun Y, et al. The phosphatase PAC1 acts as a T cell suppressor and attenuates host antitumor immunity. *Nat Immunol*. 2020; 21:287-297.
36. Holmes D, Yeh J, Yan D, et al. Dusp5 negatively regulates IL-33-mediated eosinophil survival and function. *EMBO J*. 2015;34: 218-235.
37. Al-Chami E, Tormo A, Pasquin S, et al. Interleukin-21 administration to aged mice rejuvenates their peripheral T-cell pool by triggering de novo thymopoiesis. *Aging Cell*. 2016;15:349-360.
38. Hirose J, Masuda H, Tokuyama N, et al. Bone resorption is regulated by cell-autonomous negative feedback loop of Stat5-Dusp axis in the osteoclast. *J Exp Med*. 2014;211:153-163.
39. Roskoski R. ERK1/2 MAP kinases: structure, function, and regulation. *Pharmacol Res*. 2012;66:105-143.
40. Kidger A, Rushworth L, Stellzig J, et al. Dual-specificity phosphatase 5 controls the localized inhibition, propagation, and transforming potential of ERK signaling. *Proc Natl Acad Sci USA*. 2017;114:E317-E326.
41. Kutty RG, Talipov MR, Bongard RD, et al. Dual specificity phosphatase 5-substrate interaction: a mechanistic perspective. *Compr Physiol*. 2017;7:1449-1461.
42. Moon S, Lim M, Park J, et al. Dual-specificity phosphatase 5 attenuates autoimmune arthritis in mice via reciprocal regulation of the Th17/Treg cell balance and inhibition of osteoclastogenesis. *Arthritis Rheumatol*. 2014;66:3083-3095.
43. Wu Z, Xu L, He Y, et al. DUSP5 suppresses interleukin-1β-induced chondrocyte inflammation and ameliorates osteoarthritis in rats. *Aging*. 2020;12:26029-26046.
44. Wang W, Liao P, Shen M, et al. SCP1 regulates c-Myc stability and functions through dephosphorylating c-Myc Ser62. *Oncogene*. 2016; 35:491-500.
45. Keyse S. Dual-specificity MAP kinase phosphatases (MKPs) and cancer. *Cancer Metastasis Rev*. 2008;27(2):253-261.
46. Kidger A, Keyse S. The regulation of oncogenic Ras/ERK signalling by dual-specificity mitogen activated protein kinase phosphatases (MKPs). *Semin Cell Dev Biol*. 2016;50(50):125-132.
47. Jeffrey K, Camps M, Rommel C, et al. Targeting dual-specificity phosphatases: manipulating MAP kinase signalling and immune responses. *Nat Rev Drug Discov*. 2007;6:391-403.
48. Zhang Y, Blattman JN, Kennedy NJ, et al. Regulation of innate and adaptive immune responses by MAP kinase phosphatase 5. *Nature*. 2004;430:793-797.
49. Fuentealba L, Eivers E, Ikeda A, et al. Integrating patterning signals: Wnt/GSK3 regulates the duration of the BMP/Smad1 signal. *Cell*. 2007;131:980-993.
50. Gomez-Puerto M, Iyengar P, García de Vinuesa A, et al. Bone morphogenetic protein receptor signal transduction in human disease. *J Pathol*. 2019;247:9-20.
51. Hill C. Turning off Smads: identification of a Smad phosphatase. *Dev Cell*. 2006;10:412-413.
52. Kim K, Kim D, Lee D, et al. Peroxiredoxin II negatively regulates BMP2-induced osteoblast differentiation and bone formation via PP2A Cα-mediated Smad1/5/9 dephosphorylation. *Exp Mol Med*. 2019;51:1-11.
53. Kokabu S, Nojima J, Kanomata K, et al. Protein phosphatase magnesium-dependent 1A-mediated inhibition of BMP signaling is independent of Smad dephosphorylation. *J Bone Miner Res*. 2010;25:653-660.
54. Liu X, Chai J, Ou X, Li M, Liu Z. Structural insights into substrate selectivity, catalytic mechanism, and redox regulation of rice photosystem II core phosphatase. *Mol Plant*. 2019;12:86-98.
55. Nil Z, Hervás R, Gerbich T, et al. Amyloid-like assembly activates a phosphatase in the developing *Drosophila* embryo. *Cell*. 2019;178: 1403-1420.
56. Mcconnell JL, Wadzinski BE. Targeting protein serine/threonine phosphatases for drug development. *Mol Pharmacol*. 2009;75:1249-1261.
57. Ducruet A, Vogt A, Wipf P, et al. Dual specificity protein phosphatases: therapeutic targets for cancer and Alzheimer's disease. *Annu Rev Pharmacol Toxicol*. 2005;45:725-750.
58. Krzyzosiak A, Sigurdardottir A, Luh L, et al. Target-based discovery of an inhibitor of the regulatory phosphatase PPP1R15B. *Cell*. 2018; 174:1216-1228.
59. Chiang D, Lebesgue N, Beavers D, et al. Alterations in the interactome of serine/threonine protein phosphatase type-1 in atrial fibrillation patients. *J Am Coll Cardiol*. 2015;65:163-173.

SUPPORTING INFORMATION

Additional supporting information may be found online in the Supporting Information section at the end of this article.

How to cite this article: Liu X, Liu X, Du Y, et al. DUSP5 promotes osteogenic differentiation through SCP1/2-dependent phosphorylation of SMAD1. *Stem Cells*. 2021;39 (10):1395–1409. https://doi.org/10.1002/stem.3428